Accepted Manuscript

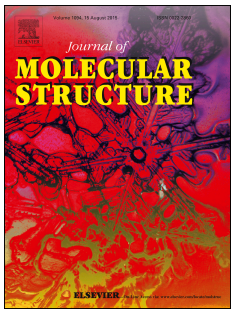

Highly functionalized dispiro oxindole-pyrrolo[1,2-*c*]thiazole-piperidone hybrid: Synthesis, characterization and theoretical investigations on the regiochemistry

Raju Suresh Kumar, Abdulrahman I. Almansour, Natarajan Arumugam, Saied M. Soliman, Raju Ranjith Kumar, Hazem A. Ghabbour

PII: S0022-2860(16)30507-5

DOI: 10.1016/j.molstruc.2016.05.061

Reference: MOLSTR 22575

To appear in: *Journal of Molecular Structure*

Received Date: 22 March 2016

Revised Date: 14 May 2016

Accepted Date: 17 May 2016

Please cite this article as: R. Suresh Kumar, A.I. Almansour, N. Arumugam, S.M. Soliman, R. Ranjith Kumar, H.A. Ghabbour, Highly functionalized dispiro oxindole-pyrrolo[1,2-*c*]thiazole-piperidone hybrid: Synthesis, characterization and theoretical investigations on the regiochemistry, *Journal of Molecular Structure* (2016), doi: 10.1016/j.molstruc.2016.05.061.

Highly functionalized dispiro oxindole–pyrrolo[1,2-*c*]thiazole–piperidone hybrid: Synthesis, characterization and theoretical investigations on the regiochemistry

Raju Suresh Kumar,[a,*] Abdulrahman I. Almansour,[a] Natarajan Arumugam,[a] Saied M. Soliman,[b,c] Raju Ranjith Kumar,[d,*] Hazem A.Ghabbour[e,f]

The synthesis of highly functionalized dispiro oxindole–pyrrolo[1,2-*c*]thiazole–piperidone hybrid has been achieved regioselectively employing microwave-assisted three-component 1,3-dipolar cycloaddition. Structural elucidation of the compound has been accomplished using NMR spectroscopy and further confirmed by single crystal X-ray crystallographic studies. The cycloaddition was found to proceed by normal electronic demand (NED) character with a significant high charge transfer (0.1247eV) from the 1,3-dipole to the dipolarophile. The regiochemistry has been explained using the local reactivity descriptors obtained from the DFT calculations. The DFT optimized molecular structure agreed well with the X-ray results.

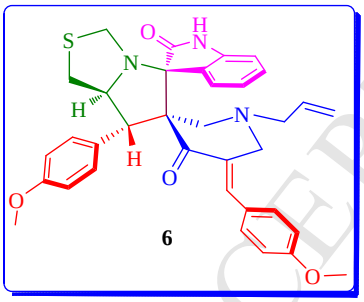

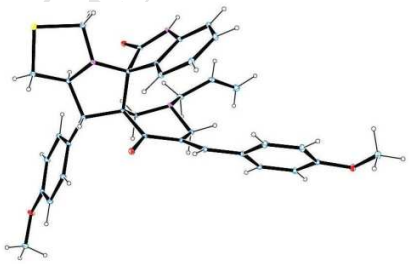

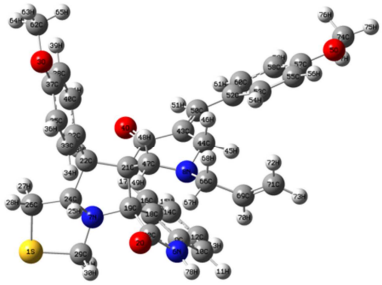

Highly functionalized dispiro oxindole-pyrrolo[1,2-*c*]thiazole-piperidone hybrid: Synthesis, characterization and theoretical investigations on the regiochemistry

Raju Suresh Kumar,[a,*] Abdulrahman I. Almansour,[a] Natarajan Arumugam,[a] Saied M. Soliman,[b,c] Raju Ranjith Kumar,[d,*] Hazem A.Ghabbour[e,f]

[a]*Department of Chemistry, College of Science, King Saud University, P.O. Box 2455, Riyadh 11451, Saudi Arabia*
[b]*Department of Chemistry, College of Science & Arts, King Abdulaziz University, P.O. Box 344, Rabigh 21911, Saudi Arabia*
[c]*Department of Chemistry, Faculty of Science, Alexandria University, P.O. Box 426, Ibrahimia, Alexandria 21321, Egypt*
[d]*Department of Organic Chemistry, School of Chemistry, Madurai Kamaraj University, Madurai 625 021, Tamil Nadu, India*
[e]*Department of Pharmaceutical Chemistry, College of Pharmacy, King Saud University, P.O. Box 2457, Riyadh 11451, Saudi Arabia*
[f]*Department of Medicinal Chemistry, Faculty of Pharmacy, University of Mansoura, Mansoura 35516, Egypt.*

Abstract

The synthesis of highly functionalized dispiro oxindole–pyrrolo[1,2-*c*]thiazole–piperidone hybrid has been achieved regioselectively employing microwave-assisted three-component 1,3-dipolar cycloaddition. Structural elucidation of the compound has been accomplished using NMR spectroscopy and further confirmed by single crystal X-ray crystallographic studies. The molecular structure of the compound crystallized in monoclinic, $P2_1/c$, a = 11.6182 (2) Å, b = 12.2466 (2) Å, c = 21.7061 (3) Å, β = 103.018 (1)°, V = 3009.04 (8) Å^3, Z = 4. The cycloaddition was found to proceed by normal electronic demand (NED) character with a significant high charge transfer (0.1247eV) from the 1,3-dipole to the dipolarophile. The regiochemistry has been explained using the local reactivity descriptors obtained from the DFT calculations. The DFT optimized molecular structure agreed well with the X-ray results.

*Corresponding author: Tel: +91-9655591445; E-mail: raju.ranjithkumar@gmail.com (Ranjith Kumar R); Tel:+966-4675907; fax: +966-4675992; E-mail: sraju@ksu.edu.sa, drrajusureshkumar@gmail.com (Suresh Kumar R);

Introduction

1,3-Dipolar cycloadditions constitute a highly versatile and prevailing tool for the construction of pharmacologically important hybrid heterocycles [1-3]. Spirooxindoles are attractive synthetic targets because of their prevalence in many natural products such as rychnophyilline [4], alstonisine [5], strychnofoline [6] and spirotryprostatin A [7] and their applications in medicine and therapeutics (Fig. 1) [4,8-9]. Spirooxindoles have also been found to target the p53−MDM2 interaction [10]. Pyrrolothiazoles are the central skeletons for numerous alkaloids and pharmacologically important compounds [11,12] and display wide array of biological activities, enabling their use as hepatoprotective [13], antibiotic [14], antidiabetic [15], anticonvulsant [16], anti-inflammatory [17], antileukemic agents [18] besides being used in the treatment for Alzheimer disease [19]. Heterocycles possessing piperidone sub-unit also gains importance as antitumor agents [20] in addition to being useful synthons for the construction of complex molecules [21]. Hence it is conceivable that the integration of piperidone, spirooxindole and pyrrolothiazole into a molecule may result in the discovery of new leads.

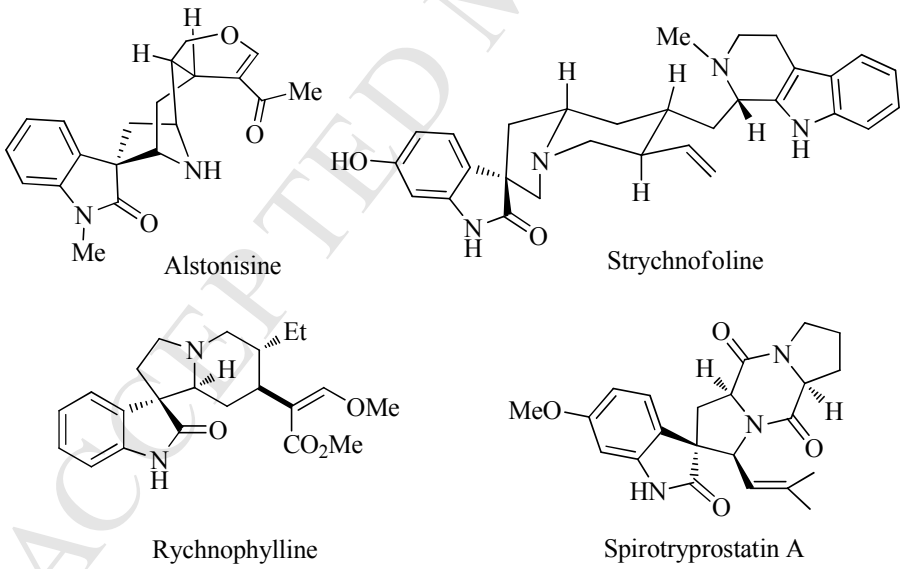

Figure 1 Representative naturally occurring spirooxindole heterocyclic hybrids

Microwave-assisted organic reactions have received much attention in recent years in view of the numerous advantages. Due to the rapid and uniform dielectric heating, it is

conceivable that microwave-assisted reactions occur in much lesser time in contrast to reactions under conventional heating and thus consequently leads to cleaner reactions with enhanced yield and fewer side products. Recently several investigations pertaining to the utility of microwave in synthetic organic chemistry have been reported, which targets wither to improve the classical organic reactions or to promote new reactions **[**22**]**. However, the utility of microwave irradiation to carry out multi-component reactions is an emerging technique.

Although the scope of 1,3-dipolar cycloaddition reaction in the synthesis of spiro compounds has been broadened by the use of different dipolarophiles [23-27], to the best of our knowledge, the utilization of compounds with piperidone sub unit embedded with three unsaturated double bonds as dipolarophlies has been less explored. As part of our ongoing investigations in the construction and/or biological screening of novel heterocycles [21,28-34], herein we report the synthesis and X-ray analysis of dispiro oxindole–pyrrolo[1,2-*c*]thiazole–piperidone hybrid. In addition we also intend to investigate the regiochemistry of the cycloaddition through DFT calculations.

Results and Discussion

Initially, the synthesis of 3,5-bis(4-methoxyphenylmethylidene)piperidin-4-one (**2**) was accomplished following a literature method [35]. Subsequently 1-allyl-3,5-bis(4-methoxyphenylmethylidene)piperidin-4-one (**3**) was prepared by the reaction of **2** with allyl chloride in acetone (Scheme 1). The structure of **3** was confirmed by NMR spectroscopic (vide supplementary) and X-ray crystallographic studies [36] (Fig. 2).

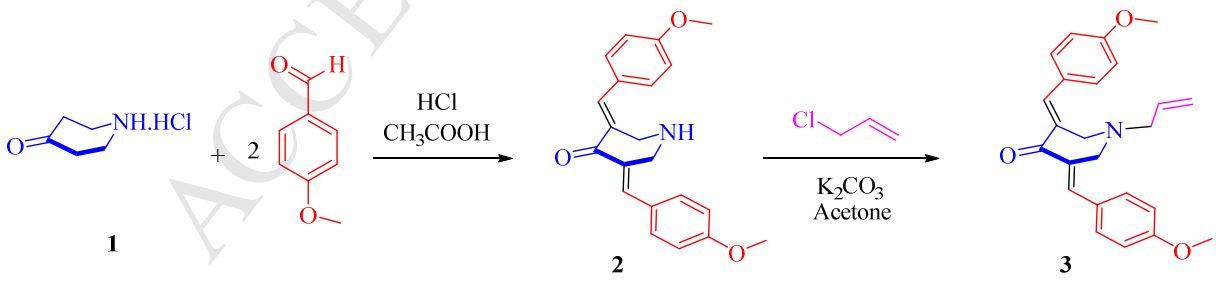

Scheme 1 Synthesis of 1-allyl-3,5-bis(4-methoxyphenylmethylidene)piperidin-4-one **3**

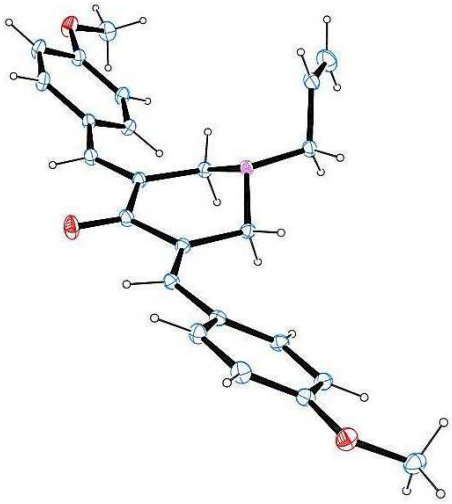

Figure 2 ORTEP diagram of **3**

Having synthesized the dipolarophile **3**, the optimization of reaction conditions for the cycloaddition was studied by taking an equimolar mixture of 1-allyl-3,5-bis(4-methoxyphenyl-methylidene)piperidin-4-one **3**, isatin **4** and thiazolidine-4-carboxylic acid **5**. The reaction in ethanol (90 min), methanol (60 min), methanol:dioxane mixture (1:1 v/v; 60 min) or dioxane (60 min) under reflux, afforded the dispiro oxindole–pyrrolo[1,2-*c*]thiazole–piperidone, **6** in 62, 70, 67 or 69 % yield, respectively. Subsequently, the same reaction was examined under microwave irradiation in a focused microwave synthesizer with a view to improve the yield and reduce the reaction time. An equimolar mixture of **3**, **4** and **5** without any solvent was irradiated with microwave at 90 ^{o}C for 10 min. The reaction mixture was extracted with ethylacetate and subjected to column chromatographic purification to obtain the product **6** in 76% isolated yield. Further, in order to ensure thorough mixing of the reactants, the same reaction was also performed after the addition of 4-5 drops of DMF. As expected, the reaction was completed in 5 minutes affording the product **6** in 85%. Apparently, an increase in the yield of the product was observed under microwave method when compared to the conventional heating.

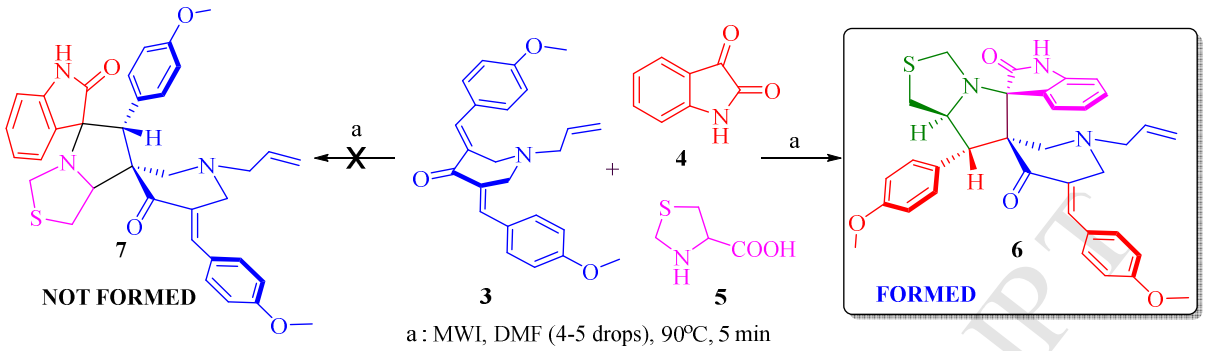

Scheme 2. Synthesis of dispiro oxindole–pyrrolo[1,2-*c*]thiazole–piperidone **6**

The structure of **6** was elucidated using elemental analysis, FT-IR, ^{1}H, ^{13}C and 2D NMR spectroscopic data. In the ^{1}H NMR spectrum of **6**, the doublet at 4.40 ppm (*J* 10.0 Hz) can be readily assigned to H-4, which show H,H-COSY correlation (vide supplementary) with the multiplet in the range 4.65-4.70 ppm assignable to H-4a. The *J* value presumably reveals that H-4 and H-4a are *trans*. The C,H-COSY correlation of H-4 and H-4a assigns the signals at 49.21 and 69.16 ppm to C-4 and C-4a respectively. This assignment is further confirmed from the DEPT 135 spectrum. Furthermore, H-4 shows HMBCs with C-3 and C-2 spiro carbons at 76.80 and 72.78 ppm, respectively apart from showing HMBCs with the carbonyl carbon C-4′ at 197.66 ppm and the *ipso* and *ortho* carbons of the *para*-methoxy phenyl ring at C-4. The H,H-COSY correlation of H-4a assigns the multiplets at 2.73-2.82 and 2.98-3.01 ppm to 5-CH_2. The doublet at 3.68 ppm (*J* 6.5 Hz) and the multiplet at 3.50-3.56 ppm is due to 7-CH_2. The doublet and the multiplet at 1.92 ppm (*J* 13.0 Hz) and 3.50-3.56 ppm are due to 2′-CH_2 protons whereas the multiplets at 2.73-2.82 ppm and 3.50-3.56 ppm are due 6′-CH_2 protons of the 4-pyridone ring. Furthermore, these protons show HMBCs with C-4′ apart from showing HMBCs with C-7′ at 60.53 ppm. The C,H-COSY correlation of C-7′ assigns the doublet of doublets at 3.15 ppm (*J* 13.5, 4.5 Hz) and the multiplet at 2.73-2.82 to 7′-CH_2 protons. From H,H-COSY spectrum, the multiplets at 5.59-5.67 ppm and 4.95-5.02 ppm can be assigned to H-8′ and 9′-CH_2 respectively. The NH proton of the oxindole ring appears as a singlet at 8.46 ppm and the aromatic protons appear as multiplets at 6.65-7.30 ppm. For better understanding, the ^{1}H and ^{13}C NMR chemical shift assignment of **6** are shown in Fig. 3.

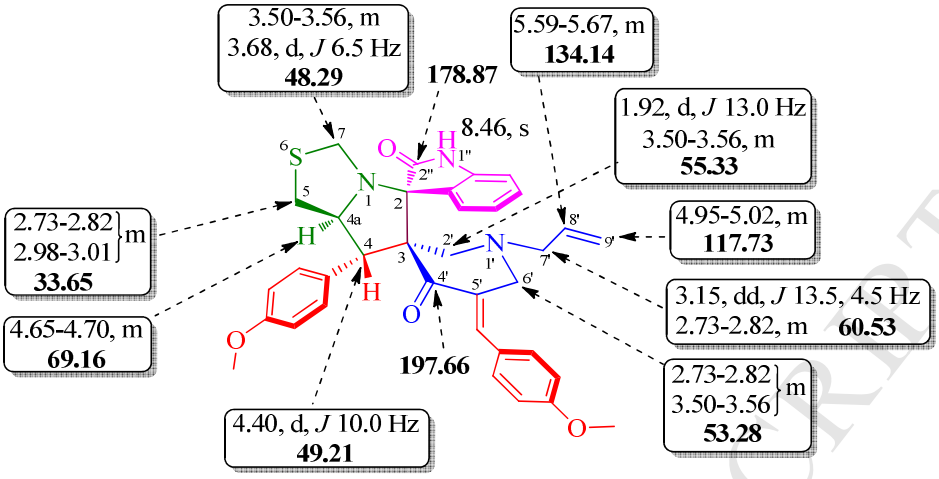

Figure 3 Selected ^{1}H and ^{13}C chemical shifts of **6**

X-ray crystallographic study of a single crystal of **6** [37] (Fig. 4) confirms the structure elucidated from NMR spectroscopic studies. The crystallographic data, conditions used for the intensity data collection and some features of the structure refinements are listed in Table 1 and the selected geometric parameters are listed in Table 2. In the crystal structure of compound **6**, the unit cell contains one independent molecule composed of a pyrrolo[1,2-*c*]thiazole ring (C7-C12/S1/C13/N2) which make dihedral angles nearly perpendicular with all spiro linked rings *viz*. oxindole ring (C1-C8/N1), pyridinone ring (C9/C20-C22/N3/C23) and phenyl ring (C14-C19) 85.68°, 84.04° and 79.67°, respectively (Fig. 4). In the crystal structure, two intermolecular N–H···O and C–H···O hydrogen bonds are observed to form a network like structure (Fig. 5 and Table 3).

Table 1 The crystal and experimental data of compound **6**

Crystal data	
Chemical formula	$C_{35}H_{35}N_3O_4S$
MW	593.72
Crystal system, space group	Monoclinic, $P2_1/c$
Temperature (K)	100
a, *b*, *c* (Å)	11.6182 (2), 12.2466 (2), 21.7061 (3)
α, β, γ (°)	103.018 (1)
V (Å3)	3009.04 (8)
Z	4

Radiation type	Mo *Kα*
μ (mm^{-1})	0.15
Crystal size (mm)	0.52 × 0.30 × 0.17
Data collection	
Diffractometer	Bruker *APEX*-II CCD diffractometer
Absorption correction	Multi-scan *SADABS* Bruker 2014
T_{min}, T_{max}	0.925, 0.974
No. of measured, independent and observed [I > 2σ(I)] reflections	38512, 9623, 7064
R_{int}	0.046
Refinement	
R[F^2 > 2σ(F^2)], wR(F^2), S	0.053, 0.132, 1.03
No. of reflections	9623
No. of parameters	394
No. of restraints	0
H-atom treatment	H atoms treated by a mixture of independent and constrained refinement
$\Delta\rho_{max}$, $\Delta\rho_{min}$ (e $Å^{-3}$)	0.39, −0.36

Table 2 Selected geometric parameters (Å, °) of compound **6**

S1—C12	1.8340 (16)	N1—C1	1.4046 (19)
S1—C13	1.8377 (17)	N1—C8	1.3540 (19)
O1—C8	1.2322 (18)	N2—C7	1.4665 (18)
O2—C17	1.3655 (19)	N2—C11	1.4650 (19)
O2—C31	1.434 (2)	N2—C13	1.4523 (19)
O3—C20	1.2230 (19)	N3—C22	1.465 (2)
O4—C28	1.3645 (18)	N3—C23	1.4602 (19)
O4—C35	1.430 (2)	N3—C32	1.465 (2)
C12—S1—C13	93.34 (7)	O1—C8—N1	125.49 (14)
C17—O2—C31	116.87 (13)	N1—C8—C7	108.60 (12)
C28—O4—C35	116.42 (13)	N2—C11—C12	104.13 (13)
C1—N1—C8	111.53 (12)	N2—C11—C10	99.98 (11)
C7—N2—C11	108.16 (11)	S1—C12—C11	103.85 (11)
C7—N2—C13	120.05 (12)	S1—C13—N2	103.73 (10)
C11—N2—C13	109.60 (11)	O2—C17—C16	115.81 (14)
C22—N3—C23	109.40 (11)	O2—C17—C18	124.40 (14)
C22—N3—C32	112.03 (12)	O3—C20—C21	121.89 (12)
C23—N3—C32	113.74 (12)	O3—C20—C9	120.73 (12)
N1—C1—C2	127.47 (14)	N3—C22—C21	110.45 (12)
N1—C1—C6	109.72 (12)	N3—C23—C9	107.95 (11)
N2—C7—C6	111.62 (12)	O4—C28—C27	116.14 (14)
N2—C7—C9	101.94 (10)	O4—C28—C29	123.92 (14)
N2—C7—C8	111.62 (10)	N3—C32—C33	111.94 (13)
O1—C8—C7	125.53 (13)		

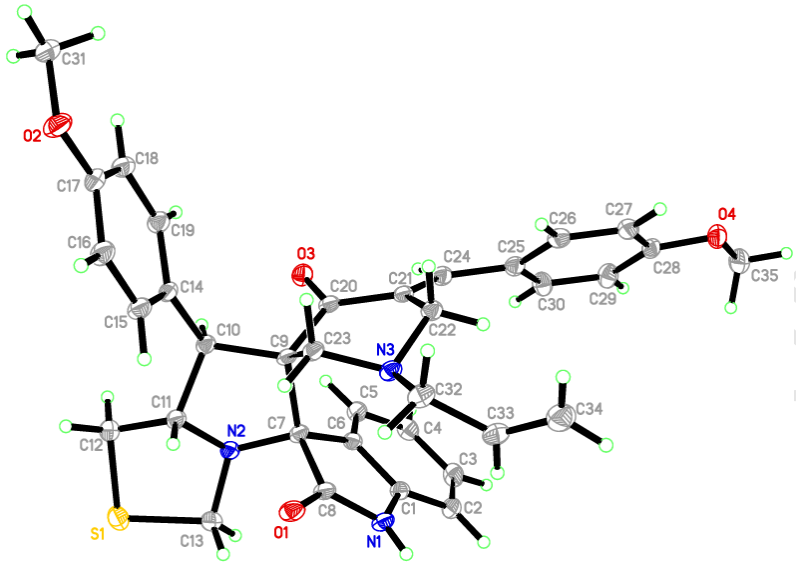

Figure 4 ORTEP diagram of **6**

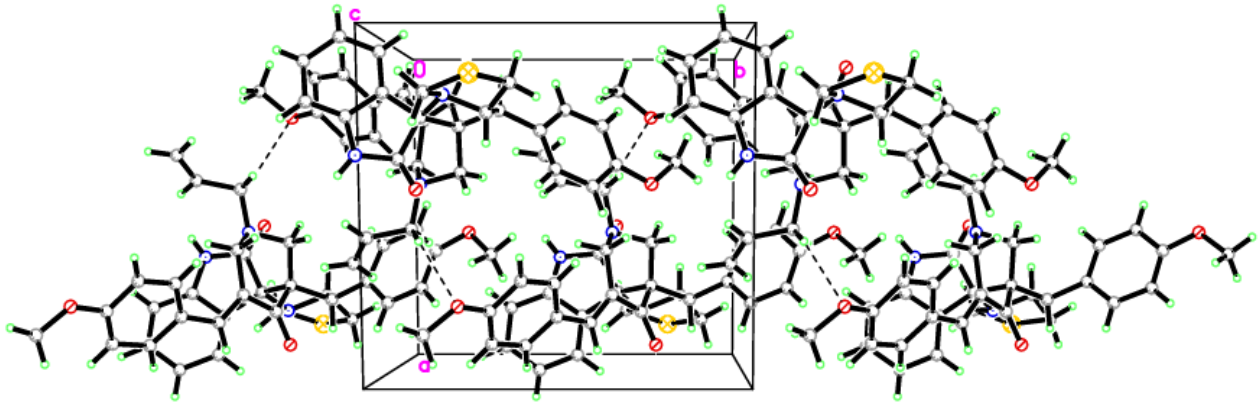

Figure 5 A view of the crystal packing of the title compound showing network structure. Dashed lines indicate weak hydrogen bonds

Table 3 Hydrogen-bond geometry (Å, °) of compound **6**

D—H···A	D—H	H···A	D···A	D—H···A
N1—H1N1···O1^{i}	0.84 (2)	2.02 (2)	2.8514 (17)	172.8 (19)
C32—H32A···O4^{ii}	0.9900	2.4600	3.179 (2)	129.00
Symmetry codes: (i) −x+1, −y, −z; (ii) −x+1, y+1/2, −z−1/2.				

A plausible reaction pathway to validate the formation of dispiro oxindole–pyrrolo[1,2-*c*]thiazole–piperidone **6** is depicted in Scheme 3. The reaction of isatin **4** and thiazolidine-4-carboxylic acid **5** by dehydration and successive decarboxylation furnishes the azomethine ylide **8**, which are known to exist in the isomeric forms **8a** and **8b**. Probably, the azomethine ylide, *viz*. **8a** undergoes cycloaddition with 1-allyl-3,5-bis(4-methoxyphenylmethylidene)piperidin-4-one **3** *via* path 1 furnishing **6**. The regioselectivity observed in the reaction may be explained by the fact that the electron-rich carbon of the 1,3-dipole **8a** prefers to add over the electron-deficient carbon of the α,β-unsaturated moiety of the dipolarophile **3**. The other possible regioisomer **7** was not observed in the reaction. In this section, a theoretical investigation of the regioselectivity of this cycloaddition reaction in the frame work of DFT calculations was performed.

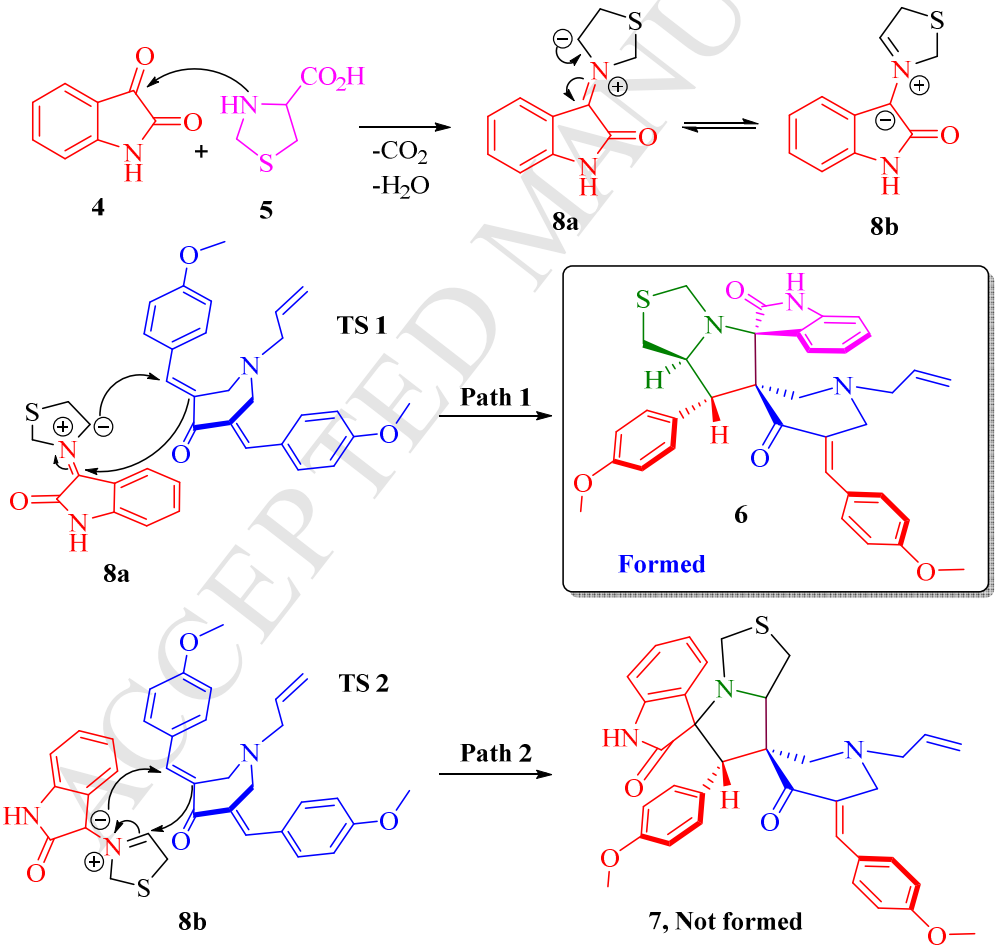

Scheme 3 Proposed mechanism for the formation of spiroheterocyclic hybrid **6**

Table 4 shows the values of the FMO energies (eV), the electronic chemical potentials and the global electrophilicity of the reactants. Figure 6 presents a schematic representation of the possible interactions between the FMOs ($HOMO_{dipole}$–$LUMO_{dipolarphile}$) and ($HOMO_{dipolarphile}$–$LUMO_{dipole}$). From Table 4 and Figure 6, we can notice that the $HOMO_{dipolarphile}$– $LUMO_{dipole}$ gap is larger (3.861 eV) than the $HOMO_{dipole}$–$LUMO_{dipolarphile}$ gap (3.024 eV). Hence the main interaction occurs between the HOMO of **8** and the LUMO of **3**. Consequently, this cycloaddition reaction has NED character. Moreover, the electronic chemical potential of **8** (-3.2770 eV) is higher than that for **3** (-3.6953 eV) indicating that charge transfer occurs from the dipole **8** to dipolarphile **3**, which is in agreement with the FMO analysis. The amount of charge transfer from the dipole **8** to dipolarophile **3** is calculated to be 0.1247e. At the transition state structure, the dipole fragment is positive while the dipolarophile is negative which confirm the NED.

Table 4 The FMO energies (E), electronic chemical potential (**μ**), nucleophilicty (N) and electrophilicity (ω) indices for the reactants.

Reactant	E_H	E_L	μ	ω	N
3	-5.5523	-1.8384	-3.6953	1.8385	3.5688
8	-4.8627	-1.6912	-3.2770	1.6930	4.2583

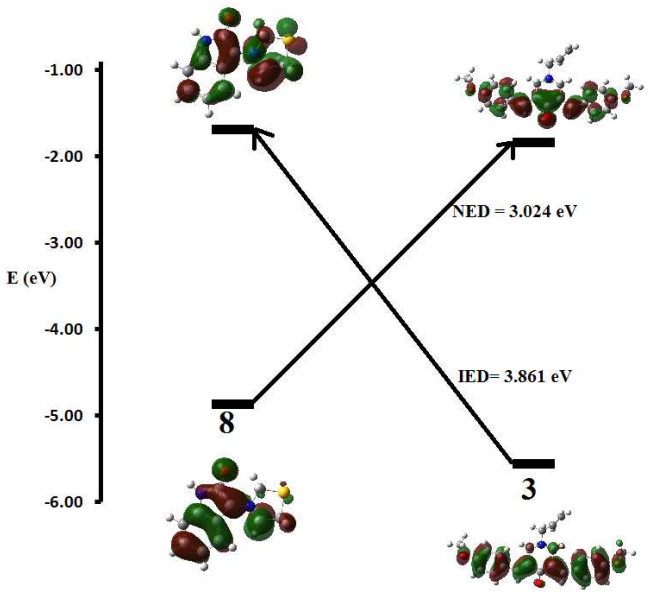

Figure 6 Possible interactions between the FMOs

Domingo *et al*. classified electrophiles based on the electrophilicity index as strong (ω> 1.50 eV), moderate (1.50 > ω > 0.80 eV) and marginal (ω< 0.80 eV). On other hand, nucleophiles could be classified as strong (N > 3.00 eV), moderate (3.00 > N > 2.00 eV) and marginal (N < 2.00 eV) [38-40]. As a result, **8** could be considered as a strong electrophile and nucleophile, whereas **3** is a strong electrophile and moderate nucleophile. Based on the values of nucleophilicity index (N) listed in Table 4, the dipole **8** has higher nucleophilicity (4.2583 eV) than the dipolarphile (3.5688eV). On other hand, the electrophilicity index (ω) of **8** (1.6930 eV) is lower than **3 (**1.8385 eV). As a result, **8** is the nucleophile while **3** is the electrophile in this reaction, in agreement with the NED character CA reaction.

The local electrophilicity indices ω_k and N_k of atom k were used to explain the regioselectivity of the studied CA reaction. The values of the Fukui indices (f_k^+ and f_k^-) and local electrophilicity indices (ω_k and N_k) are reported in Table 5. Scheme 4 depicts these interactions for better visualization. In the studied CA reaction, the most favorable two-center interaction takes place between C15 and C17 of **3** as electrophile and C16 and C8 of **8** as nucleophile, respectively. These results are in agreement with the experimental findings, which afforded **6** and not **7**.

Table 5 Electrophilic and nucleophilic Fukui indices and local electrophilicities for the reactive atoms of **3** and **8**.

Reactant	**3**			**8**	
	C15	**C17**		**C8**	**C16**
f_k^+	-0.1205	-0.0142	f_k^+	-0.0398	-0.1544
f_k^-	-0.0027	-0.0846	f_k^-	-0.1855	-0.1853
ω_k	**0.2215**	*0.0049*	N_k	*0.6575*	**0.7889**

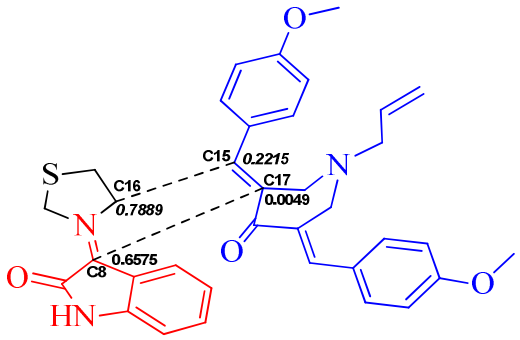

Scheme 4 Favorable interactions using local electrophilicity indices

Molecular mechanism

The above cycloaddition may presumably occur along the two regioisomeric pathways as shown in Scheme 3. The geometries of the two TSs are given in Figure 7 together with the newly forming bond lengths. Table 6 reports the energies (a.u.) and relative energies (kcal/mol). The potential energy surfaces (PESs) corresponding to all the reaction channels, are illustrated in Figure 8. Based on the calculated energy difference between the product and reactants, the product **6** is more stable thermodynamically than **7**. On other hand, the calculated activation energies of the different reaction pathways between **3** and **8** showed that the pathway **1** (adduct **6**) is the most favored kinetically in comparison with pathway **2** (product **7**). The large energy difference (10.78 Kcal/mol) between the two cycloaddition TSs confirmed that **6** is the only product that could be formed in this reaction as observed experimentally.

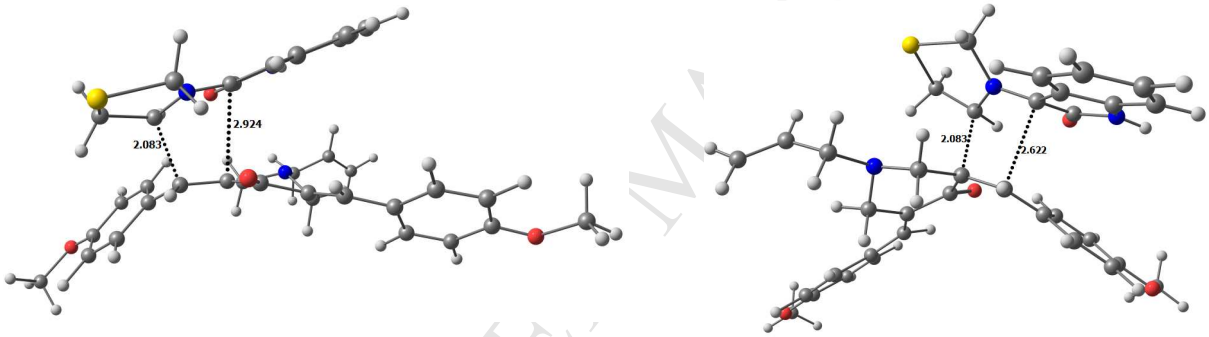

TS1 TS2

Figure 7 The four transition state structure for the CA reaction

Table 6 Energies and relative energies (ΔE) of the reactants, transition states and products.

System	E(a.u.)	ΔE (Kcal/mol)[a]
3	-1209.5491	
8	-1007.9056	
TS1	-2217.4459	5.48451
TS2	-2217.4287	16.26471
6	-2217.4864	-19.94534
7	-2217.4799	-15.83885

[a]The energies of the TSs and products are referred to the sum [E_3+E_8].

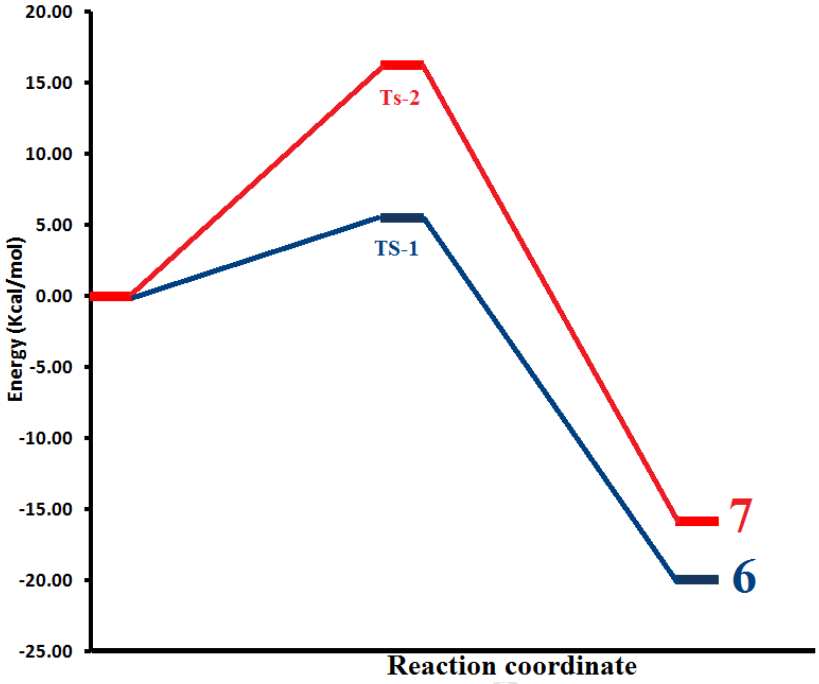

Figure 8 Energy profiles, in kcal/mol for the two pathways of the CA reactions.

Optimized molecular structure of 6

The optimized molecular structure of **6** done by using B3LYP/6-31G(d,p) is shown in Figure 9. The calculated bond distances and bond angles are given in Table 7 and Table S1 (Supplementary data). Figure 10 shows the correlations between the calculated and experimental geometric parameters (bond distances and angles). The correlation between the calculated and experimental bond distances and angles gave correlation coefficients (R^2) of 0.9963 and 0.9798, respectively. Moreover, the root mean square deviation (RMSD) of the bond distances and angles are 0.011 Å and 1.05˚, respectively. As a result, the geometric parameters are well predicted.

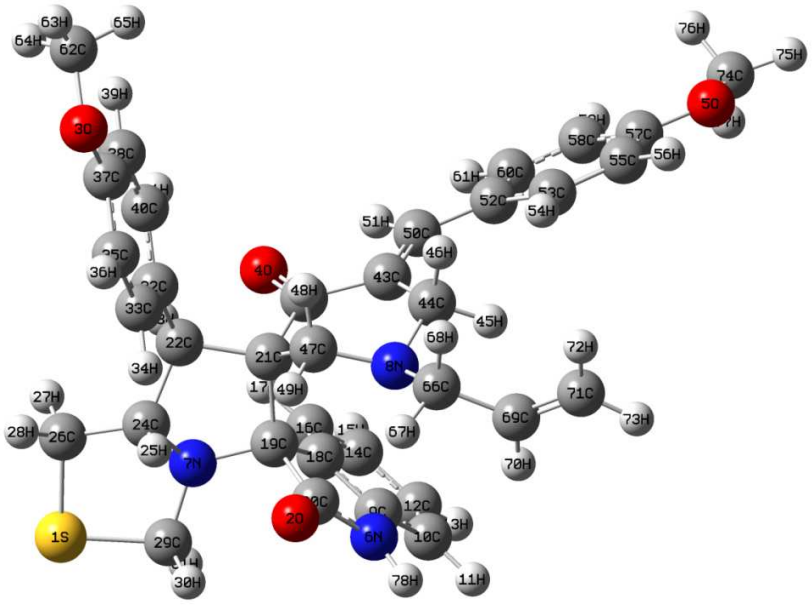

Figure 9 The optimized molecular structure of **6**

Table 7 The calculated and experimental bond distances of **6**

Parameter	Calc.	X-ray	Parameter	Calc.	X-ray
R(1-26)	1.855	1.834	R(21-42)	1.546	1.541
R(1-29)	1.860	1.838	R(21-47)	1.538	1.529
R(2-20)	1.222	1.232	R(22-24)	1.532	1.524
R(3-37)	1.367	1.366	R(22-32)	1.516	1.507
R(3-62)	1.418	1.434	R(24-26)	1.528	1.515
R(4-42)	1.228	1.223	R(32-33)	1.406	1.396
R(5-57)	1.360	1.365	R(32-40)	1.400	1.393
R(5-74)	1.421	1.430	R(33-35)	1.390	1.390
R(6-9)	1.400	1.405	R(35-37)	1.401	1.393
R(6-20)	1.377	1.354	R(37-38)	1.399	1.389
R(7-19)	1.463	1.466	R(38-40)	1.397	1.393
R(7-24)	1.456	1.465	R(42-43)	1.494	1.484
R(7-29)	1.448	1.452	R(43-44)	1.513	1.507
R(8-44)	1.459	1.464	R(43-50)	1.359	1.345
R(8-47)	1.459	1.460	R(50-52)	1.456	1.462
R(8-66)	1.466	1.465	R(52-53)	1.416	1.406
R(9-10)	1.390	1.385	R(52-60)	1.409	1.395
R(9-18)	1.404	1.391	R(53-55)	1.385	1.384
R(10-12)	1.400	1.393	R(55-57)	1.404	1.396
R(12-14)	1.396	1.390	R(57-58)	1.401	1.386
R(14-16)	1.402	1.396	R(58-60)	1.391	1.386
R(16-18)	1.389	1.389	R(66-69)	1.505	1.498
R(18-19)	1.524	1.518	R(69-71)	1.333	1.317
R(19-20)	1.571	1.562	R(2-49)	2.303	2.341
R(21-22)	1.577	1.563	R(19-21)	1.622	1.609

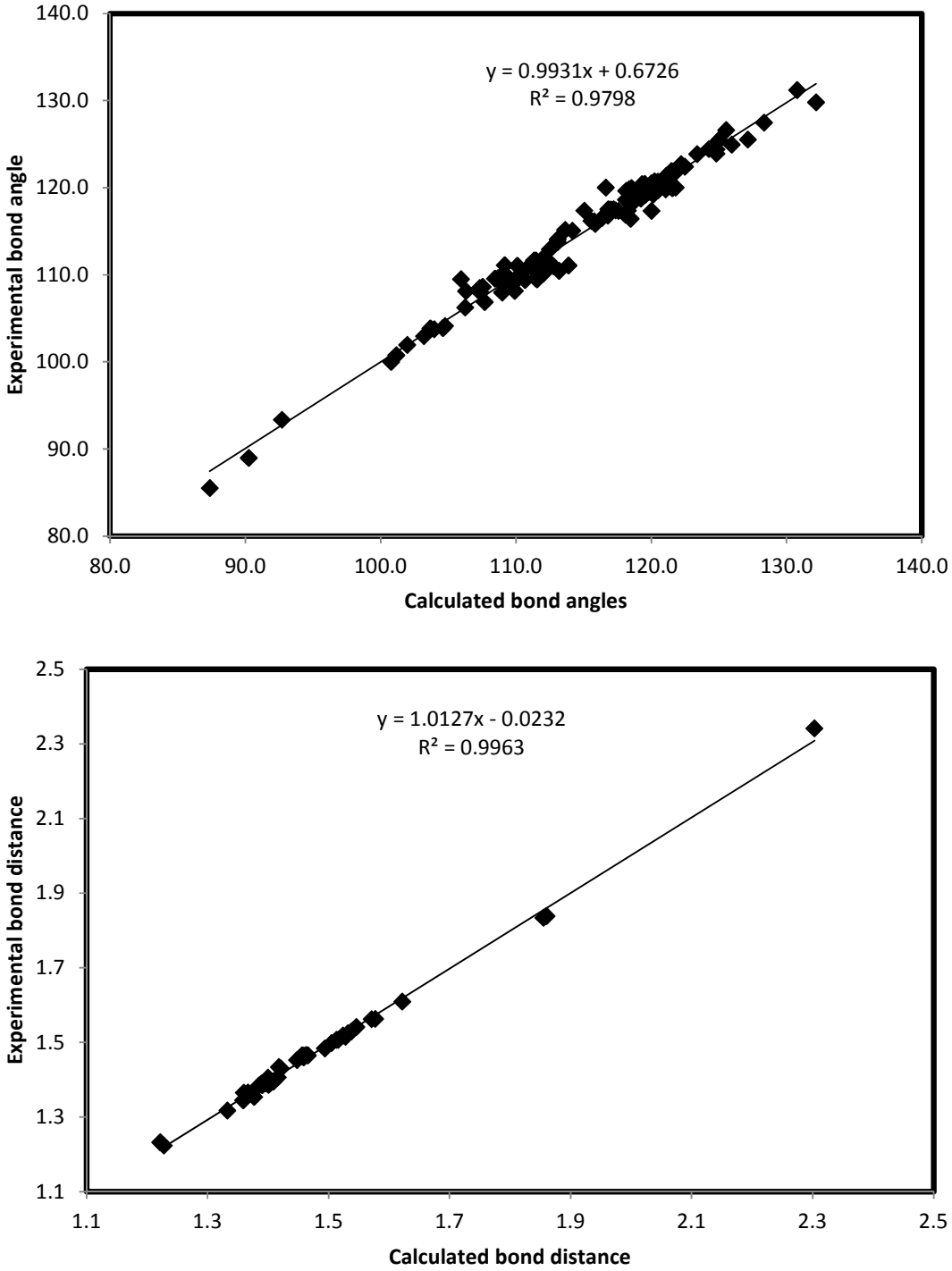

Figure 10 The correlation graphs between the calculated and experimental geometric parameters

Natural atomic charges

The charges at the different atomic sites were calculated using natural bond orbital method at the B3LYP/6-31G(d,p) method. The natural atomic charges are listed in Table 8. It could be seen that, the most negative atomic sites are oxygen and nitrogen atoms as those sites have high electronegativity. The natural charges at the O and N-atoms are in the range of -0.5120 to -0.6260 and -0.5028 to -0.6275, respectively. As a result, the C-atoms attached to these sites are expected to have the highest positive charge values. The most electropositive C-atom is C20 (+0.7030) as this carbon is bonded to two of the strong electronegative atoms. Moreover, the calculations predicted the S-atom to have electropositive nature (+0.1777). All the H-atoms have positive natural charges where the most electropositive H-site is amino group proton (H78) which has natural charge of +0.4381. A graphical representation of the charge density distribution at the different atomic site of **6** is shown in figure 11. This molecular electrostatic potential map gave indication on the reactive site for electrophilic and nucleophilic attack. The blue regions represent the regions with high electron deficiency and those are related to the reactive sites for nucleophilic attack. In contrast, the negative red regions -the most electron rich- represent the most reactive sites for electrophilic attack. As can be seen from The MEP figure shown in Fig. 11, the most reactive electrophilic sites are those related to the carbonyl O-atoms (O4 and O2) while the most nucleophilic site is the amine proton (H78). On other hand, dipole moment is an important electronic parameter which is related to the charge distribution among different atomic sites. The dipole moment of **6** is calculated to be 7.4818 Debye which indicate the high polarity of the studied compound probably due to the large number of electronegative atoms.

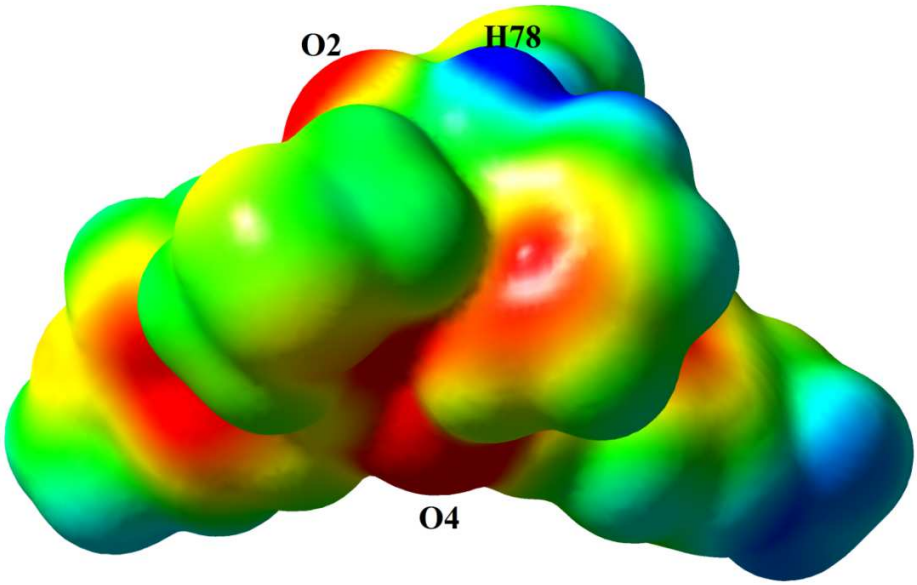

Figure 11 Molecular electrostatic potential (MEP) map of **6**

Table 8 The natural atomic charges of **6**

Atom	NAC	Atom	NAC	Atom	NAC
S 1	0.1777	H 27	0.2498	C 53	-0.1949
O 2	-0.6206	H 28	0.2608	H 54	0.2435
O 3	-0.5209	C 29	-0.3823	C 55	-0.2741
O 4	-0.5795	H 30	0.2242	H 56	0.2534
O 5	-0.5120	H 31	0.2515	C 57	0.3384
N 6	-0.6275	C 32	-0.0713	C 58	-0.3250
N 7	-0.5173	C 33	-0.2236	H 59	0.2453
N 8	-0.5028	H 34	0.2413	C 60	-0.1753
C 9	0.1752	C 35	-0.2705	H 61	0.2435
C 10	-0.2799	H 36	0.2498	C 62	-0.3276
H 11	0.2406	C 37	0.3169	H 63	0.2315
C 12	-0.2178	C 38	-0.3184	H 64	0.2057
H 13	0.2410	H 39	0.2416	H 65	0.2050
C 14	-0.2597	C 40	-0.2070	C 66	-0.2891
H 15	0.2414	H 41	0.2489	H 67	0.2619
C 16	-0.1980	C 42	0.5714	H 68	0.2057
H 17	0.2642	C 43	-0.1310	C 69	-0.2302
C 18	-0.0801	C 44	-0.2866	H 70	0.2294
C 19	0.0816	H 45	0.2555	C 71	-0.4342
C 20	0.7030	H 46	0.2092	H 72	0.2151
C 21	-0.0919	C 47	-0.2806	H 73	0.2238
C 22	-0.2686	H 48	0.2283	C 74	-0.3300
H 23	0.2854	H 49	0.2667	H 75	0.2352
C 24	-0.0584	C 50	-0.1301	H 76	0.2089
H 25	0.2344	H 51	0.2555	H 77	0.2089
C 26	-0.5795	C 52	-0.1129	H 78	0.4381

Frontier Molecular Orbitals (FMOs)

The frontier molecular orbitals; HOMO and LUMO are the outermost molecular orbital which offer a reasonable qualitative prediction of the excitation properties and the ability of electron transport [41,42]. HOMO is the higher energy orbital containing electrons and so it acts as an electron donor while LUMO is the lowest energy orbital that acts as an electron acceptor. Also, the HOMO and LUMO are very popular quantum chemical parameters which determine the molecular reactivity. The isodensity surface plots of HOMO and LUMO levels of the studied compound are drawn using the same level of theory (Fig. 12). It can be seen from figure 12 that, the electron density of HOMO is mainly localized over the thiazolidine which represent the electron donor fragment of **6**. The LUMO is localized mainly over the 4-methoxyphenyl and piperidin-4-one moieties which act as the electron acceptor fragments of **6.** The electronic transition from HOMO and LUMO could be described as π→π* in which the electron flow takes place from the thiazolidine π–molecular orbitals to the π*-molecular orbitals of the 4-methoxyphenyl and piperidin-4-one moieties. The HOMO and LUMO energies are -5.6021 and -1.8373 eV, respectively and hence the minimum energy of the electronic transition is 3.7647 eV. The energies of HOMO and LUMO are negative, which indicates that the studied compound is stable molecule [43].

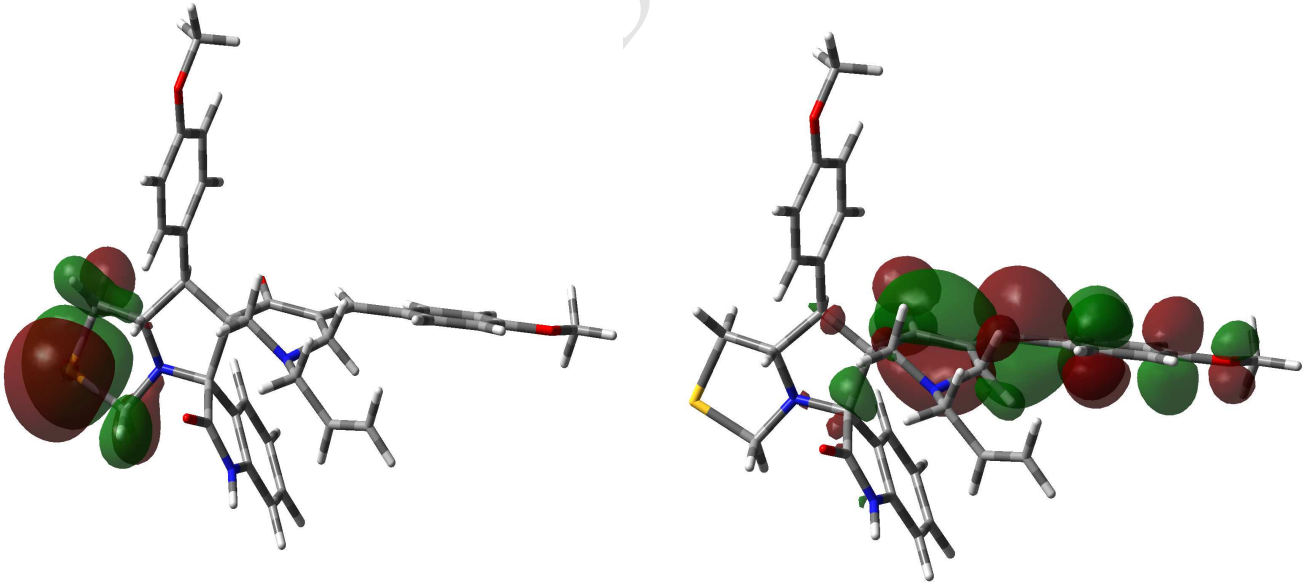

HOMO **LUMO**

Figure 12 The isodensity surface plots of HOMO and LUMO levels of **6**

Experimental

General methods

Chemistry

Melting points were recorded using open capillary tubes and are uncorrected. The ^{1}H, ^{13}C and 2-D NMR spectra were recorded on a Bruker 400 or 500 MHz instruments (Faellanden, Switzerland) in $CDCl_3$ using TMS as internal standard. Standard Bruker software was used throughout. Chemical shifts are given in parts per million (δ-scale) and the coupling constants are given in Hertz. IR spectra were recorded on a Perkin Elmer system 2000 FT IR instrument (KBr) (Shelton, AL, USA). Elemental analyses were performed on a Perkin Elmer 2400 Series II Elemental CHNS analyzer (Waltham, MA, USA).

*Synthesis of (3E,5E)-1-allyl-3,5-bis(4-methoxyphenylmethylidene)piperidin-4-one (**3**)*

A equimolar mixture of (3*E*,5*E*)-3,5-bis(4-methoxyphenylmethylidene)piperidin-4-one (0.023 g), allyl chloride (0.100 g) and K_2CO_3 (0.041 g) in 30 mL of acetone was stirred at room temperature for 30 minutes. After completion of the reaction as evident from TLC, the excess solvent was removed under vacuum and the crude product was extracted with ethyl acetate and recrystallized from the same to afford the product as a yellow solid, (92%); Mp 97-99 ^{o}C; ^{1}H NMR (400 MHz, $CDCl_3$): δ_H 3.21 (d, 2H, *J*=6.4 Hz, 7'-CH_2), 3.76-3.87 (m, 10H, 2'-CH_2, 6'-CH_2 and 2xOCH_3), 5.12 (d, 1H, *J*=10.4 Hz, 9'-CH_2), 5.22 (d, 1H, *J*=17.2 Hz, 9'-CH_2), 5.78–5.85 (m, 1H, H-8'), 6.93 (d, 2H, *J*=8.8 Hz, ArH), 7.35 (d, 2H, *J*=8.8 Hz, ArH), 7.78 (s, 2H, arylmethylidene). ^{13}C NMR (100 MHz, $CDCl_3$): δ_C 55.00, 55.71, 60.95, 114.50, 118.89, 128.41, 131.77, 132.73, 135.01, 136.49, 160.65, 187.60. Anal. calcd for $C_{24}H_{25}NO_3$: C, 76.77; H, 6.71; N, 3.73%; found: C, 76.95; H, 6.57; N, 3.81%.

*General procedure for the synthesis of spiro[2.3"]oxindole-spiro[3.3']-1'-allyl-5'-(4-methoxyphenylmethylidene)tetrahydro-4'(1H)-pyridinone-4-(4-methoxyphenyl)hexahydro-pyrrolo[1,2-c]thiazole (**6**).*

An equimolar mixture of (3*E*,5*E*)-1-allyl-3,5-bis(4-methoxyphenylmethylidene)piperidin-4-one **3**, isatin **4** and thiazolidine-4-carboxylic acid **5** with 4-5 drops of DMF was irradiated in a CEM microwave synthesizer at 90 ^{o}C for 5 minutes. After completion of the reaction (TLC), water (50 mL) was added to the reaction mixture and extracted with ethyl acetate (3x30 mL). The excess

solvent was evaporated under reduced pressure. The resultant solid was dried in vacuum and crystallized from ethyl acetate to obtain pure **6** as colorless solid, (84%); Mp 147-149 ^{o}C; IR (KBr) ν_{max} 1608, 1620, 1631, 1708, 3390 cm^{-1}; ^{1}H NMR (500 MHz, $CDCl_3$): δ_H 1.92 (d, 1H, *J*=13.0 Hz, 2'-CH_2), 2.73-2.82 (m, 3H, 5-CH_2, 6'-CH_2, 7'-CH_2), 2.98–3.01 (m, 1H, 5-CH_2), 3.15 (dd, 1H, *J*=13.5, 4.5 Hz, 7'-CH_2), 3.50-3.56 (m, 3H, 7-CH_2, 2'-CH_2, 6'-CH_2), 3.68 (d, 1H, *J*=6.5 Hz, 7-CH_2), 3.79 (s, 3H, OCH_3), 3.80 (s, 3H, OCH_3), 4.40 (d, 1H, *J*=10.0 Hz, H-4), 4.65–4.70 (m, 1H, H-4a), 4.95-5.02 (m, 2H, 9'-CH_2), 5.59–5.67 (m, 1H, H-8'), 6.66 (d, 1H, *J*=7.5 Hz, ArH), 6.79–6.81 (m, 3H, Ar-H and arylmethylidene), 6.84 (d, 2H, *J*=8.0 Hz, ArH), 6.94 (d, 2H, *J*=8.0 Hz, ArH), 6.97 (d, 1H, *J*=8.0 Hz, ArH), 7.12 (t, 1H, *J*=7.5 Hz, ArH), 7.26-7.30 (m, 3H, ArH), 8.46 (s, 1H, 1''-NH). ^{13}C NMR (125 MHz, $CDCl_3$): δ_C 33.65, 48.25, 49.21, 53.29, 55.23, 55.28, 55.33, 60.53, 69.16, 71.60, 72.78, 109.04, 113.81, 117.73, 121.72, 126.01, 127.67, 128.38, 129.10, 129.16, 130.35, 131.46, 131.97, 134.14, 137.19, 141.43, 158.63, 160.06, 178.87, 197.66. Anal. calcd for $C_{35}H_{35}N_3O_4S$: C, 70.80; H, 5.94; N, 7.08%; found: C, 70.98; H, 5.81; N, 7.21%.

X-ray details

The compound **6** was obtained as single crystals by slow evaporation from ethyl acetate solution of the pure compound at room temperature. Data were collected on a Bruker APEX-II CCD diffractometer, equipped with graphite monochromatic Mo Kα radiation, λ = 0.71073 Å at 100 (2) K. Cell refinement and data reduction were carried out by Bruker SAINT. SHELXT [44, 45] was used to solve structure. The final refinement was carried out by full-matrix least-squares techniques with anisotropic thermal data for nonhydrogen atoms on *F*. CCDC 1450952 contains the supplementary crystallographic data for this compound can be obtained free of charge from the Cambridge Crystallographic Data Centre via www.ccdc.cam.ac.uk/data_request/cif.

Computational details

Full geometry optimizations were carried out for the reactants, transition states (TSs) and cycloaddition products (CAs) using the DFT with the B3LYP [46, 47] functional and the 6-31G(d,p) basis set. All calculations were carried out with GAUSSIAN 03 [48]. The stationary points were characterized by frequency calculations in order to verify that minima and transition states have zero and one imaginary frequency, respectively. Each TS gave one negative vibrational mode corresponding to the motion involving the formation of the newly forming C–C bonds. The vibrational mode was assigned appropriately by means of visual inspection and

animation using the Gaussview software [49]. The reported total energies include zero point energy (ZPE) corrections are given at 298.15 K. Analysis of the frontier molecular orbital (FMO) interactions, global electrophilicity index (ω), was calculated following the expression [50-53], $\omega = (\mu^2/2\eta)$, where μ is the electronic chemical potential, $\mu = (E_H + E_L)/2$, and η is the chemical hardness, $\eta = (E_L - E_H)$. The nucleophilicity index, N [51], which is defined as $N = E_{H(Nu)} - E_{H(TCE)}$, where tetracyanoethylene (TCE) is chosen as the reference [54,55]. The atomic electronic population and DFT-based reactivity indices were computed using natural population analysis (NPA) [56]. The local electrophilicity ω_k and nucleophilicity N_k indices of atom k are obtained by the help of Fukui index (f_k) using equations:

$$\omega_k = \omega f_k^+ = \omega[Q_k(N+1) - Q_k(N)]$$

$$N_k = N f_k^- = \omega[Q_k(N) - Q_k(N-1)]$$

Where $q_k(N)$, $q_k(N+1)$, $q_k(N-1)$ are the gross electronic population of site k in neutral, anionic, and cationic systems, respectively [57]. The optimized structure of **3** and **8** are given in figure S9 (Supplementary data).

Conclusions

A sustainable microwave-assisted three-component 1,3-dipolar cycloaddition reaction has been developed for the regioselective synthesis of highly functionalized dispiro oxindole–pyrrolo[1,2-*c*]thiazole–piperidone hybrid **6**. In order to rationalize the formation of **6**, theoretical calculation was performed. The results of the DFT calculations showed that the azomethine ylide; **8** and the dipolarophile **3** act as strong nucleophile and electrophile, respectively wherein the amount of charge transfer from **8** to **3** at the TS structure is 0.1247eV. The CAs reaction has normal electronic demand (NED). The local reactivity indices (ω_k and N_k) as well as the transition state calculations indicated the regioselective formation of **6** is the most favored. The high activation energy difference between the TSs suggested that the thermodynamically stable product **6** is the only product that could be obtained, in agreement with experimental results.

Acknowledgments

The authors acknowledge the Deanship of Scientific Research at King Saud University for Research Grant No. RGP-026.

References

1. A. Padwa, Synthetic Applications of 1,3-Dipolar Cycloaddition Chemistry toward Heterocycles and Natural Products; John Wiley & Sons, 2002.
2. R. Grigg, M. A. B. Sarker, Tetrahedron 62 (2006) 10332-10343.
3. L. Yulin, L. Bin, L. Xiaofang, L. Xianyong, Ziran Kexueban 25 (2010) 101-103.
4. C. Marti, E. M. Carreira, Eur. J. Org. Chem. 12 (2003) 2209-2219.
5. R. L. Garnick, P. W. Le Quesne, J. Am. Chem. Soc. 1978, 100, 4213-4219.
6. R. Bassleer, M. C. Depauw-Gillet, B. Massart, J.-M. Marnette, P. Wiliquet, M. Caprasse, L. Angenot, Planta Med. 1982, 45, 123-126.
7. M. Zhang, W.-L. Wang, Y.-C. Fang, T.-J. Zhu, Q.-Q. Gu, W.-M. Zhu, J. Nat. Prod. 71 (2008) 985-989.
8. B. M. Trost, M. K. Brennan, Synthesis 18 (2009) 3003-3025.
9. C. V. Galliford, K. A. Scheidt, Angew. Chem., Int. Ed. 46 (2007) 8748-8758.
10. S. Yu, D. Qin, S. Shangary, J. Chen, G. Wang, K. Ding, D. McEachern, S. Qiu, Z. Nikolovska-Coleska, R. Miller, S. Kang, D. Yang, S. Wang, J. Med. Chem. 52 (2009) 7970-7973.
11. P. Prasanna, K. Balamurugan, S. Perumal, P. Yogeeswari, D. Sriram, Eur. J. Med. Chem. 45 (2010) 5653-5661.
12. S. V. Karthikeyan, B. D. Bala, V. P. A. Raja, S. Perumal, P. Yogeeswari, D. Sriram, Bioorg. Med. Chem. Lett. 20 (2010) 350-353.
13. M. Hasegawa, A. Nakayama, S. Yokohama, T. Hosokami, Y. Kurebayashi, T. Ikeda, Y. Shimoto, S. Ide, Y. Honda, N. Suzuki, Chem. Pharm. Bull. 43 (1995) 1125-1131.
14. J. E. Baldwin, R. T. Freeman, C. Lowe, C. J. Schofield, E. Lee, Tetrahedron 45 (1989) 4537-4550.
15. T. D. Aicher, B. Balkan, P. A. Bell, L. J. Brand, S. H. Cheon, R. O. Deems, J. B. Fell, W. S. Fillers, J. D. Fraser, J. Gao, D. C. Knorr, G. G. Kahle, C. L. Leone, J. Nadelsen, R. Simpson, H. C. Smith, J. Med. Chem. 41 (1998) 4556-4566.
16. G. Trapani, M. Franco, A. Latrofa, G. Genchi, M. Brigiani, M. Mazzoccoli, M. Persichella, M. Serra, G. Biggio, G. Liso, Eur. J. Med. Chem. 29 (1994) 197-204.
17. T. Burgemeister, G. Dannhadt, E. Graf, R. Obergrusberger, Arch. Pharm. 320 (1987) 799-806.

18. J. B. Jones, J. M. Young, J. Med. Chem. 11 (1968) 1176-1182.
19. D. E. Butler, J. D. Leonard, B. W. Caprathe, Y. J. L. Italien, M. R. Pavia, F. M. Hershenson, P. H. Poschel, J. G. Marriott, J. Med. Chem. 30 (1987) 498-503.
20. Y. Santiago-Vazquez, S. Das, U. Das, E. Robles-Escajeda, N. M. Ortega, C. Lema, A. Varela-Ramírez, R. J. Aguilera, J. Balzarini, E. D. Clercq, S. G. Dimmock, D. K. J. Gorecki, J. R. Dimmock, Eur. J. Med. Chem. 77 (2014) 315-322.
21. R. Suresh Kumar, A. I. Almansour, N. Arumugam, J. C. Menéndez, H. Osman, R. R. Kumar, Synthesis 47 (2015) 2721-2730.
22. M. Adib, A. H. Jahromi, N. Tavoosi, M. Mahdavi, H. R. Bijanzadeh, Tetrahedron Lett. 47 (2006) 2965-2967.
23. V. Rajkumar, N. A. Aslam, C. Reddy, S. A. Babu, Synlett 4 (2012) 549-556.
24. A. R. S. Babu, R. Raghunathan, Tetrahedron Lett. 48 (2007) 6809−6813.
25. R. Jain, K. Sharma, D. Kumar, Tetrahedron Lett. 53 (2012) 1993−1997.
26. K. Zhao, S. L. Zhu, D. Q. Shi, X. P. Xu, S. J. Ji, Synthesis 11 (2010) 1793-1803.
27. J. M. Yang, Y. Hu, Q. Li, F. Yu, J. Cao, D. Fang, D. Q. Shi, ACS. Comb. Sci. 16 (2014) 139−145.
28. A.I. Almansour, R. Suresh Kumar, N. Arumugam, A. Basiri, Y. Kia, M.A. Ali, M. Farooq, V. Murugaiyah, Molecules 20 (2015) 2296-2309.
29. R. Suresh Kumar, A.I. Almansour, N. Arumugam, A. Basiri, Y. Kia, R. Ranjith Kumar, Aust. J. Chem. 68 (2015) 863–871.
30. N. Arumugam, A.I. Almansour, R. Suresh Kumar, J.C. Menéndez, M.A. Sultan, U. Karama, H. A. Ghabbour, H.-K. Fun, Molecules 20 (2015) 16142-16153.
31. A.I. Almansour, R. Suresh Kumar, N. Arumugam, A. Basiri, Y. Kia, M.A. Ali, BioMed Research International Volume 2015, Article ID 965987, 9 pages.
32. A.I. Almansour, R. Suresh Kumar, F. Beevi, A.N. Shirazi, H. Osman, R. Ismail, T.S. Choon, B. Sullivan, K. McCaffrey, A. Nahhas, K. Parang, M.A. Ali, Molecules 19 (2014) 10033-10055.
33. R. Suresh Kumar, A. I. Almansour, N. Arumugam, M.A. Ali, Medicinal Chemistry 10 (2014) 228-236.
34. Kumar, R. S.; Ramar, A.; Perumal, S.; Almansour, A. I.; Arumugam, N.; Ali, M. A. Synth. Commun. 43 (2013) 2763-2772.

35. J. R. Dimmock, M. P. Padmanilayam, R. N. Puthucode, A. J. Nazarali, N. L. Motaganahalli, G. A. Zello, J. W. Quail, E. O. Oloo, H. B. Kraatz, J. S. Prisciak, T. M. Allen, C. L. Santos, J. Balzarini, E. De Clercq, E. K. Manavathu, J. Med. Chem. 44 (2001) 586-593.
36. A. I. Almansour, R. Suresh Kumar, N. Arumugam, R. Vishnupriya and J. Suresh, Acta Cryst. E69 (2013) o1071.
37. Crystallographic data (including structure factors) for the compound **6** have been deposited with the Cambridge Crystallographic Data Centre as supplementary publication number CCDC 1450952. Copies of the data can be obtained, free of charge, on application to CCDC, 12 Union Road, Cambridge CB2 1EZ, UK [fax: +44 (0)1223 336033 or e-mail: deposit@ccdc.cam.ac.uk].
38. L.R. Domingo, M.J. Aurell, P. Perez, R. Contreras, Tetrahedron 58 (2002) 4417-4423.
39. L.R. Domingo, P. Perez, Org. Biomol. Chem. 11 (2013) 4350-4358.
40. P. Jaramillo, L.R. Domingo, E. Chamorro, P. Perez, J. Mol. Struct. THEOCHEM 865 (2008) 68-72.
41. M. Belletete, J.F. Morin, M. Leclerc, G. Durocher, J. Phys. Chem. A, 109 (2005)6953-6959.
42. D. Zhenminga, S. Hepinga, L. Yufanga, L. Dianshenga, L. Bob, SpectrochimicaActa Part A, 78 (2011) 1143-1148.
43. S.W. Xia, X. Xu, Y.L. Sun, Y.L. Fan, Y.H. Fan, C.F. Bi, D.M. Zhang, L.R. Yang, Chin. J. Struct. Chem., 25 (2006) 849-853.
44. Sheldrick, G. M. Acta. Cryst. A 71.1 (2015) 3-8.
45. Brucker. APEX2, SAINT and SADABS. Brucker AXS Inc., Madison, Wisconsin, USA, 2009.
46. A.D. Becke, Phys. Rev. A 38 (1988) 3098-3100.
47. C. Lee, W. Yang, R.G. Parr, Phys. Rev. B 37 (1988) 785-789.
48. Frisch, M. J.; Trucks, G. W.; Schlegel, H. B.; Scuseria, G. E.; Robb, M. A.; Cheeseman, J. R.; Montgomery, J. A. Jr.; Vreven, T.; Kudin, K. N.; Burant, J. C.; Millam, J. M.; Iyengar, S. S.; Tomasi, J.; Barone, V.; Mennucci, B.; Cossi, M.; Scalmani, G.; Rega, N.; Petersson, G. A.; Nakatsuji, H.; Hada, M.; Ehara, M.; Toyota, K.; Fukuda, R.; Hasegawa, J.; Ishida, M.; Nakajima, T.; Honda, Y.; Kitao, O.; Nakai, H.; Klene, M.; Li, X.; Knox, J.

E.; Hratchian, H. P.; Cross, J. B.; Bakken, V.; Adamo, C.; Jaramillo, J.; Gomperts, R.; Stratmann, R. E.; Yazyev, O.; Austin, A. J.; Cammi, R.; Pomelli, C.; Ochterski, J. W.; Ayala, P. Y.; Morokuma, K.; Voth, G. A.; Salvador, P.; Dannenberg, J. J.; Zakrzewski, V. G.; Dapprich, S.; Daniels, A. D.; Strain, M. C.; Farkas, O.; Malick, D. K.; Rabuck, A. D.; Raghavachari, K.; Foresman, J. B.; Ortiz, J. V.; Cui, Q.; Baboul, A. G.; Clifford, S.; Cioslowski, J.; Stefanov, B. B.; Liu, G.; Liashenko, A.; Piskorz, P.; Komaromi, I.; Martin, R. L.; Fox, D. J.; Keith, T.; Al-Laham, M. A.; Peng, C. Y.; Nanayakkara, A.; Challacombe, M.; Gill, P. M. W.; Johnson, B.; Chen, W.; Wong, M. W.; Gonzalez, C.; Pople, J. A. GAUSSIAN 03, Revision D.01; Gaussian: Wallingford, CT, 2004.

49. GaussView, Version 4.1, R. Dennington II, T. Keith, J. Millam, Semichem Inc., Shawnee Mission, KS, (2007).
50. R.G. Parr, L. von Szentpaly, S. Liu, J. Am. Chem. Soc. 121 (1999) 1922-1924.
51. R.G. Parr, R.G. Pearson, J. Am. Chem. Soc. 105 (1983) 7512-7516.
52. R.G. Parr, W. Yang, Density Functional Theory of Atoms and Molecules, Oxford University, New York, 1989.
53. W. Kohn, L. Sham, J. Phys. Rev. 140 (1965) A1133-A1135.
54. L.R. Domingo, E. Chamorro, P. Pérez, J. Org. Chem. 72 (2008) 4615-4624.
55. L.R. Domingo, P. Pérez, Org. Biomol. Chem. 9 (2011) 7168-7175.
56. Reed, A. E.; Weinhold, F. J. Chem. Phys. 78 (1983) 4066-4073.
57. L. R. Domingo, M. J. Aurell, P. Pérez, R. Contreras, J. Phys. Chem. A 106 (2002) 6871-6875.

- Highly functionalized dispiro oxindole–pyrrolo[1,2-*c*]thiazole–piperidone hybrid has been achieved regioselectively
- Structure was accomplished using NMR spectroscopy and X-ray crystallographic studies
- The formation of product has been explained using the local reactivity descriptors obtained from the DFT calculations
- DFT optimized molecular structure agree well with the X-ray results